

Dynamic Performance of a Three-Wheeled Vehicle Steering System, Part 1: Steering System Incorporating Directional Control Valve

M. T. Heshmat^{*}, M. Abdel-Aziz[†], M. Galal Rabie[‡], M. Sabry Dwidar[§]

Abstract: During taxing, the aircraft can be treated as a three wheeled vehicle. This work deals with the dynamic behavior of this three-wheeled vehicle during the steering mode. Conventionally the hydraulic power steering systems incorporate either hydraulic or electro-hydraulic servo-systems. Nevertheless, Part 1 of this paper deals with the dynamic behavior of a steering system incorporating three directional control valves of poppet type in one housing. A nonlinear mathematical model of the directional control valve assembly was developed and used to simulate the valves dynamic behavior. The validity of the simulation program was evaluated in the steady state by comparing simulation results with results of experimental work conducted on the studied valves. The construction of the mechanical parts is explained and the kinematics of the steering system was analyzed and presented. The transient response of the steering system incorporating the directional control valve assembly was calculated, presented and discussed.

Keywords: Steering, 3-wheeled, vehicle, hydraulic, electrohydraulic, directional, control, valve, modeling, simulation, dynamic, experimental.

Nomenclature

| | |
|------------|--|
| A_p | Piston side area, m ² |
| A_{1Pp} | Poppet area subjected to inlet pressure for DCV-1, m ² |
| A_{1Ppm} | Maximum poppet area subjected to inlet pressure for DCV-1, m ² |
| A_{1Pt} | Throttling area for DCV-1 pressure side, m ² |
| A_{1Tp} | Poppet area subjected to return pressure for DCV-1, m ² |
| A_{1Tpm} | Maximum poppet area subjected to return pressure for DCV-1, m ² |
| A_{1Tt} | Throttling area for DCV-1 return side, m ² |
| B | Bulk modulus of oil, Pa |
| C_d | Discharge coefficient |
| d_1 | Diameter of the circular poppet seats for pressure and return sides for DCV-1, m |
| d_{1P} | Diameter of the circular poppet area subjected to the inlet pressure for DCV-1, m |
| d_{1T} | Diameter of the circular poppet area subjected to the return pressure for DCV-1, m |
| F_{1P} | Reaction force in the pressure side seat for DCV-1, N |

^{*} Egyptian Armed Forces, Egypt.

[†] Dr. Eng., Faculty of Engineering, Ain Shams University, Cairo, Egypt.

[‡] Professor of Mech. Engineering, Modern Academy for Engineering and Technology, Cairo, Egypt.

[§] Professor, Faculty of Engineering, Ain Shams University, Cairo, Egypt.

| | |
|---------------|--|
| F_{rf} | Rolling resistance force in the front tire, N |
| F_{S1} | Solenoid force for DCV-1, N |
| F_{1T} | Reaction force in the return side seat for DCV-1, N |
| f_{rr} | Coefficient of rolling resistance |
| f_v | Equivalent plunger friction coefficient, N.s/m |
| f_{vp} | Piston friction coefficient, N.s/m |
| I_{zz} | Mass moment of inertia of the front wheel around the steering axis, $kg.m^2$ |
| K_{sP} | Equivalent seat material stiffness for pressure side, N/m |
| K_{sT} | Equivalent seat material stiffness for return side, N/m |
| k_{vs} | Valve spring stiffness, N/m |
| L_s | Horizontal distance between steering axis and wheel center, m |
| m | Total mass of the poppet and plunger, kg |
| m_{red} | Reduced mass of the moving and rotating parts, kg |
| m_p | Reduced mass of the piston, kg |
| P_A | Pressure at the actuator cylinder chamber (A), Pa |
| P_{AB} | Pressure difference between ports (A) and (B) of the DCV assembly, Pa |
| P_B | Pressure at the actuator cylinder chamber (B), Pa |
| P_P | Pressure at the supply line, Pa |
| P_S | Pressure at the inner chamber (S), Pa |
| P_T | Pressure at the return line (T), Pa |
| Q_{1P} | Inlet flow rate to DCV-1, m^3/s |
| Q_{1T} | Exit flow rate from DCV-1 to return line, m^3/s |
| R_{sP} | Equivalent seat material damping for pressure side, N.s/m |
| R_{sT} | Equivalent seat material damping for Return side, N.s/m |
| r_{1b} | Spherical poppet radius for DCV-1, m |
| r_{re} | The radius between cylinder rod end (2) center and the shock strut center, m |
| r_{rm} | Steering load arm, m |
| s_1 | Poppet stroke for DCV-1, m |
| V_A | Volume of oil in cylinder chamber (A), m^3 |
| V_{Ao} | Initial volume of oil in cylinder chamber (A), m^3 |
| V_B | Volume of oil in cylinder chamber (B), m^3 |
| V_{Bo} | Initial volume of oil in cylinder chamber (B), m^3 |
| V_S | Volume of oil in the inner chamber (S), m^3 |
| W_f | Normal load on the front wheel assembly, N |
| x_1 | Poppet displacement for DCV-1, m |
| x_{1P} | Poppet displacement from DCV-1 pressure side seat, m |
| x_{1T} | Poppet displacement from DCV-1 return side seat, m |
| x_{o1} | Spring pre-compression distance for DCV-1, m |
| x_f | Longitudinal fixed axis of the front wheel |
| Y | Steering cylinder piston displacement, m |
| y_f | Lateral fixed axis of the front wheel |
| z_f | Normal fixed axis of the front wheel |
| Z | Pedal displacement, m |
| α_{1P} | Poppet cone vertex angle for DCV-1 pressure side, rad |
| α_{1T} | Poppet cone vertex angle for DCV-1 return side, rad |
| Δ | Steering angle, rad |
| P | Oil density, kg/m^3 |

Abbreviations

| | |
|-----|---------------------------|
| DCV | Directional control valve |
| E | Electric solenoid |
| cg | Center of gravity |

Subscripts

| | |
|---|-----------|
| 1 | for DCV-1 |
| 2 | for DCV-2 |
| 3 | for DCV-3 |

1. Introduction

During flight, takeoff and landing, the motion of aircraft is governed by the aerodynamic forces and is described by the flight mechanics rules. On the other hand, during taxing, the aircraft is actually a three wheeled vehicle. This work deals with the dynamic performance of this three-wheeled vehicle of large mass and high center of gravity with no driving torques on the wheels. The stability of these types of vehicles is very critical and needs highest considerations, particularly during the turning maneuvers. The dynamics of this class of vehicles during steering is governed by different aspects of its design, loading and operating parameters. Factors such as the road surface, weather conditions, steering speed and tire inflation pressure, play an important role, [1]. The handling qualities play a crucial part in safety and ride comfort.

The coupling between electrical and hydraulic power systems leads to much powerful steering system that saves energy and cost, [2]. Using steer by wire system have the advantages of the hydraulic systems such as the maximum power to weight ratio, high stiffness of hydraulic actuators, high controllability and precision [3]. In the steer-by-wire system, the steering wheel is connected to the steering mechanism by an electric wire rather than a shaft. A steer-by-wire system has only electrical signals connection between the steering wheel subsystem and the steering mechanism subsystem, [4]. The elimination of the steering column shaft frees up backing space, improve crash worthiness, and increase design flexibility by allowing engineers to place the steering wheel on the right or left side of the cockpit, [5].

The studied system, Figs. 1 and 2, is a hydro mechanical steering system electrically controlled by the steering pedals. The steering cylinder steers the front wheel of a three-wheeled vehicle. The operating fluid under the hydraulic generator pressure (P_P) is delivered to the steering DCV assembly. The pilot pushes an electric push button to energize the DCV-1 so the fluid flows to the DCV-2 and the DCV-3.

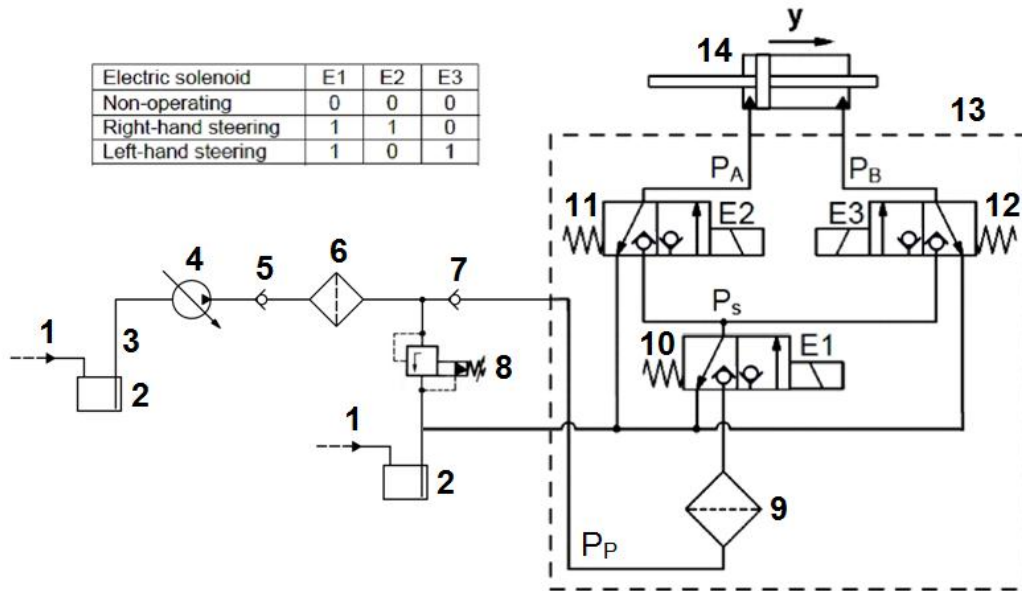
When the pilot pushes the left or the right pedal, the control circuit compares input signal received from the pedal displacement and a feedback signal from the feedback potentiometer according to the cylinder position (y). The circuit sends a steer left or right command signal according to which pedal is pushed. The magnitude of the pedal displacement (z) determines the magnitude of the steering actuator displacement (y). The control circuit energizes the DCV-2 or the DCV-3, porting a pressurized hydraulic fluid to one of the cylinder chambers to steer a left or right turn accordingly.

2. System Description and Mathematical Modeling**2.1 Hydraulic Circuit of the Steering System**

The hydraulic circuit of the studied steering system is shown in Fig.1. It consists of a hydraulic generator, a symmetrical hydraulic cylinder, (14), and a DCV assembly (13). The supply pressure (P_P) is kept practically constant due to the effect of the pump controller, considering the high pump flow rate and the very low flow demands of the steering system. The switching positions for right-hand and left-hand steering modes are illustrated in Fig. 1.

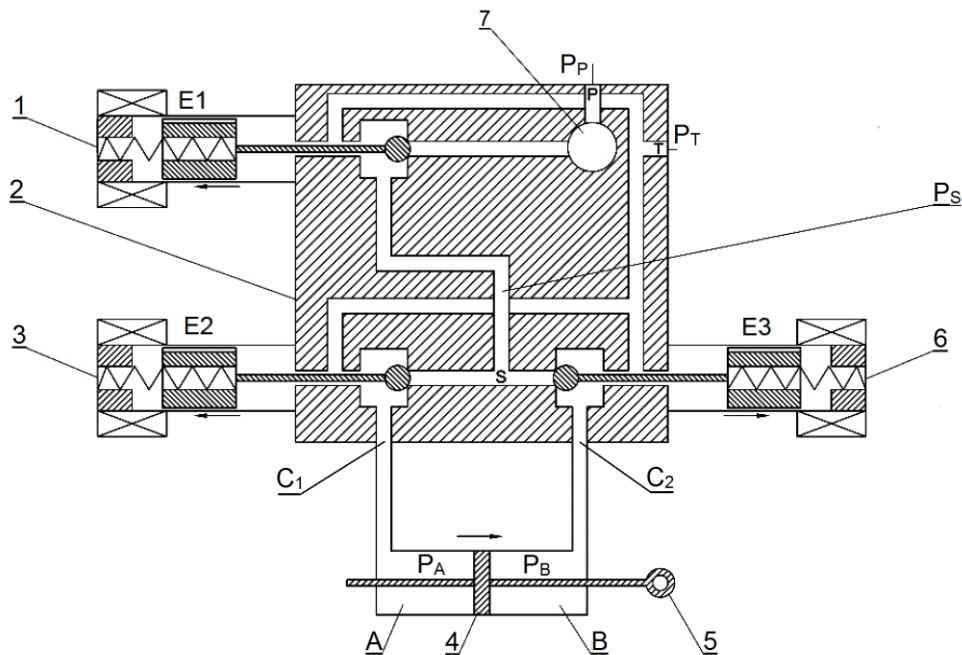
2.2 Directional Control Valve Assembly

Figure 2. shows the construction of the DCV assembly, which includes three direct operated 3/2 poppet type DCVs. By energizing solenoids (E1) and (E2), the pressure line is communicated to the left chamber of the steering cylinder, through the inlet filter (9), the DCV-2, while the right chamber is connected to the return line through the DCV-3. The steering cylinder piston moves to the left by energizing solenoids (E1) and (E3). It stops moving by de-energizing the three solenoids.



1. Tank pressurization line, 2. Tank, 3. Pump suction line, 4. Pump, 5. Check valve, 6. Filter, 7. Check valve, 8. Relief valve, 9. Inlet filter, 10. DCV-1, 11. DCV-2, 12. DCV-3, 13. DCV assembly, 14. Cylinder.

Fig. 1. Hydraulic circuit of the steering system



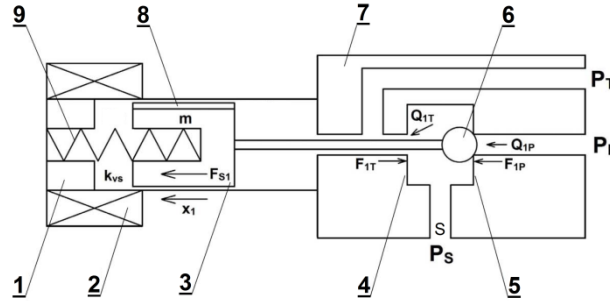
1. DCV-1, 2. Steering DCV assembly, 3. DCV-2, 4. Actuator, 5. Rod end, 6. DCV-3, 7. Filter.

Fig. 2. Schematic of the hydraulic components of the steering system

2.3 Mathematical Model of the DCV-1

Figure 3, shows a schematic of the DCV-1. The mathematical model describing the dynamic behavior of the DCV assembly is deduced considering the following assumptions:

- Neglect the transient period of the solenoid force building.
- The pressure losses in the inner transmission lines are negligible compared with the losses in the poppet valve throttling orifice.
- Neglect the axial component of pressure forces due to the pressure in the service line.
- Both of the inlet pressure (P_P) and return pressure (P_T) are constant.



1. Spring housing, 2. E1, 3. Plunger, 4. Return Side Seat, 5. Pressure Side Seat, 6. Spherical poppet, 7. Valve Housing, 8. V shape recess, 9. Spring.

Fig. 3. Schematic diagram of the DCV-1

The following are the equations describing the dynamic behavior of the DCV-1.

Equation of Motion of the Poppet

The motion of the poppet of the DCV-1 is governed by the pressure, seat reaction, solenoid, spring, damping and inertia forces, Eq. 1.

$$P_P A_{1Pp} - P_T A_{1Tp} + F_{1P} + F_{S1} - F_{1T} = m \ddot{x}_1 + f_v \dot{x}_1 + k_{vs}(x_1 + x_{o1}) \quad (1)$$

Seat Reaction Forces

The displacement of the spherical poppet (6), Fig. 3, in both the closure and the opening directions is limited mechanically. When reaching its seats, a seat reaction force takes place due to the action of the seat stiffness and structural damping of the seats materials, Eq. 2, [6].

$$F_{1P} = \begin{cases} 0 & s_1 > x_1 > 0 \\ K_{sP} |x_1| - R_{sP} \frac{dx_1}{dt} & x_1 < 0 \end{cases} \quad (2)$$

The reaction force of the right seat (F_{1P}) takes place only when (E1) is not energized. Hence, the poppet (6), and the plunger (3), are in extreme right position and the DCV-1 is fully closed, otherwise this force equals to zero, as stated by Eq. 2.

$$F_{1T} = \begin{cases} K_{sT} |x_1 - s_1| + R_{sT} \frac{dx_1}{dt} & x_1 > s_1 \\ 0 & s_1 > x_1 > 0 \end{cases} \quad (3)$$

The left seat reaction force (F_{1T}), takes place only when (E1) is energized, so that the poppet (6), and the plunger (3), are in the extreme left position and the DCV-1 is fully open. Otherwise this force equals to zero, as given by Eq. 3.

Poppet area subjected to Pressure (P_P)

When the poppet (6), rests against its right seat (5), the valve is fully closed. The contact line is a circle of diameter (d_1), Fig. 4, and the poppet area subjected to the pressure force is (A_{1Ppm}), Eq. 4.

$$A_{1Ppm} = \frac{\pi}{4} d_1^2 \quad (4)$$

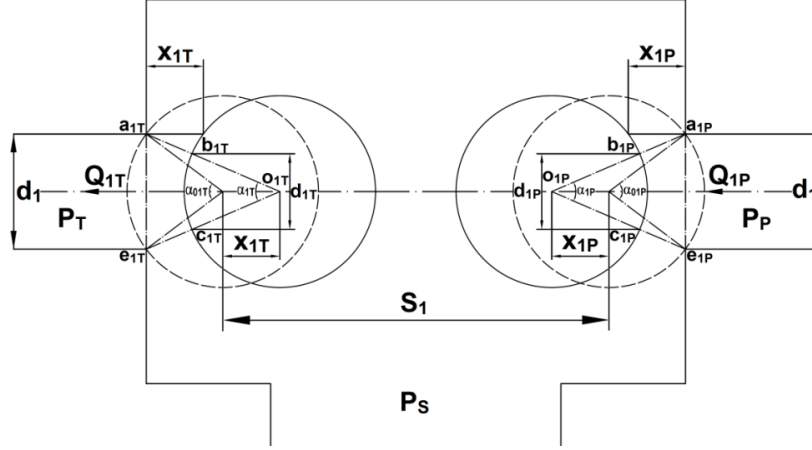


Fig. 4. Poppet valve dimensions and areas of the DCV-1

If the spherical poppet (6) is displaced by a distance (x_{1P}), the fluid is allowed to flow through the opened area. This area consists of the side area of the truncated cone ($a_{1P}b_{1P}c_{1P}e_{1P}$), whose right base area is of diameter (d_1), and left base area is of diameter (d_{1P}). The area (A_{1Pp}) is:

$$\alpha_{o1P} = 2\sin^{-1} \left(\frac{d_1}{2r_{1b}} \right) \quad (5)$$

where;

$$\alpha_{1P} = 2\tan^{-1} \left[\frac{d_1}{2\{r_{1b} \cos(\alpha_{o1P}/2) + x_{1P}\}} \right] \quad (6)$$

$$d_{1P} = 2r_{1b} \sin \left(\frac{\alpha_{1P}}{2} \right) \quad (7)$$

$$A_{1Pp} = \frac{\pi}{4} d_{1P}^2 = \pi r_{1b}^2 \sin^2 \left(\frac{\alpha_{1P}}{2} \right) \quad (8)$$

Poppet area subjected to Pressure (P_T)

$$A_{1Tpm} = \frac{\pi}{4} d_1^2 \quad (9)$$

$$\alpha_{o1T} = 2\sin^{-1} \left(\frac{d_1}{2r_{1b}} \right) \quad (10)$$

$$\alpha_{1T} = 2\tan^{-1} \left[\frac{d_1}{2\{r_{1b} \cos(\alpha_{o1T}/2) + x_{1T}\}} \right] \quad (11)$$

$$d_{1T} = 2r_{1b} \sin \left(\frac{\alpha_{1T}}{2} \right) \quad (12)$$

$$A_{1Tp} = \frac{\pi}{4} d_{1T}^2 = \pi r_{1b}^2 \sin^2 \left(\frac{\alpha_{1T}}{2} \right) \quad (13)$$

Throttling Area at the Pressure Side Seat (A_{1Pt})

The throttling area of the poppet valve, created between the poppet and right seat (A_{1Pt}), is calculated as follows:

$$\overline{a_{1P}b_{1P}} = \frac{d_1}{2 \sin(\alpha_{1P}/2)} - r_{1b} \quad (14)$$

$$A_{1Pt} = \frac{\pi}{2} (d_1 + d_{1P}) \overline{a_{1P}b_{1P}} = \frac{\pi}{2} \left[d_1 + 2r_{1b} \sin \left(\frac{\alpha_{1P}}{2} \right) \right] \left\{ \frac{d_1}{2 \sin(\alpha_{1P}/2)} - r_{1b} \right\} \quad (15)$$

The relation between poppet displacement and throttling and pressure areas of DCV-1 is shown in Fig. 5.

Throttling Area of the Return Side Seat (A_{1Tt})

$$\overline{a_{1T}b_{1T}} = \frac{d_1}{2 \sin(\alpha_{1T}/2)} - r_{1b} \quad (16)$$

$$A_{1Tt} = \frac{\pi}{2} (d_1 + d_{1T}) \overline{a_{1T}b_{1T}} = \frac{\pi}{2} \left[d_1 + 2r_{1b} \sin \left(\frac{\alpha_{1T}}{2} \right) \right] \left\{ \frac{d_1}{2 \sin(\alpha_{1T}/2)} - r_{1b} \right\} \quad (17)$$

$$Q_{1P} = C_d A_{1Pt} \sqrt{2(P_P - P_S)/\rho} \quad (18)$$

$$Q_{1T} = C_d A_{1Tt} \sqrt{2(P_S - P_T)/\rho} \quad (19)$$

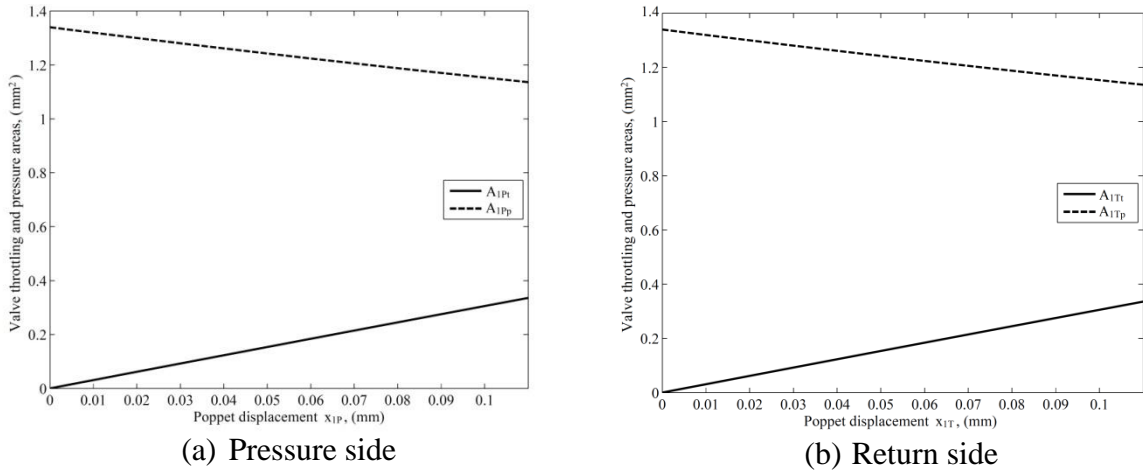


Fig. 5. Relation between poppet displacement and throttling and pressure areas of DCV-1

2.4 Mathematical Model of the DCV-2

Considering Figs. 6 and 7, the equations describing the DCV-2 were deduced on the basis of the assumptions and procedure followed in the DCV-1.

$$P_S A_{2Pp} - P_T A_{2Tp} + F_{2P} + F_{S2} - F_{2T} = m \ddot{x}_2 + f_v \dot{x}_2 + k_{vs} (x_2 + x_{o2}) \quad (20)$$

$$F_{2P} = \begin{cases} 0 & s_2 > x_2 > 0 \\ K_{sP} |x_2| - R_{sP} \frac{dx_2}{dt} & x_2 < 0 \end{cases} \quad (21)$$

$$F_{2T} = \begin{cases} K_{sT}|x_2 - s_2| + R_{sT} \frac{dx_2}{dt} & x_2 > s_2 \\ 0 & s_2 > x_2 > 0 \end{cases} \quad (22)$$

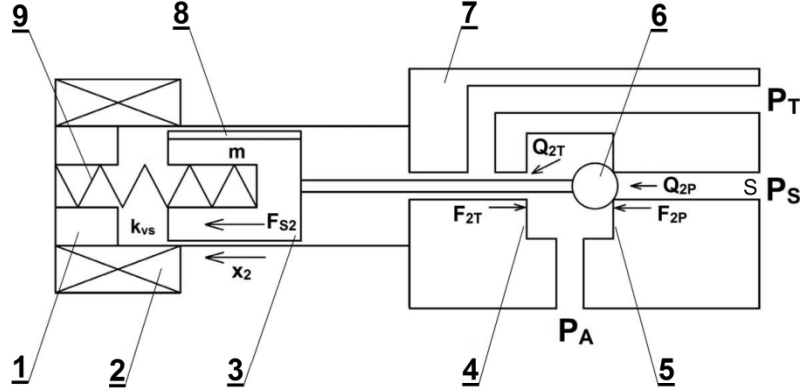


Fig. 6. Schematic diagram of the DCV-2

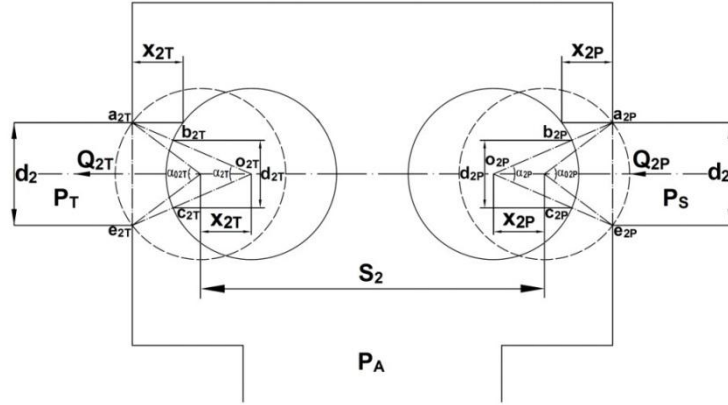


Fig. 7. Poppet valve dimensions and areas of the DCV-2

$$A_{2Ppm} = \frac{\pi}{4} d_2^2 \quad (23)$$

$$\alpha_{o2P} = 2 \sin^{-1} \left(\frac{d_2}{2r_{2b}} \right) \quad (24)$$

$$\alpha_{2P} = 2 \tan^{-1} \left[\frac{d_2}{2\{r_{2b} \cos(\alpha_{o2P}/2) + x_{2P}\}} \right] \quad (25)$$

$$d_{2P} = 2r_{2b} \sin \left(\frac{\alpha_{2P}}{2} \right) \quad (26)$$

$$A_{2Pp} = \frac{\pi}{4} d_{2P}^2 = \pi r_{2b}^2 \sin^2 \left(\frac{\alpha_{2P}}{2} \right) \quad (27)$$

$$A_{2Tpm} = \frac{\pi}{4} d_2^2 \quad (28)$$

$$\alpha_{o2T} = 2 \sin^{-1} \left(\frac{d_2}{2r_{2b}} \right) \quad (29)$$

$$\alpha_{2T} = 2 \tan^{-1} \left[\frac{d_2}{2\{r_{2b} \cos(\alpha_{o2T}/2) + x_{2T}\}} \right] \quad (30)$$

$$d_{2T} = 2r_{2b} \sin\left(\frac{\alpha_{2T}}{2}\right) \quad (31)$$

$$A_{2Tp} = \frac{\pi}{4} d_{2T}^2 = \pi r_{2b}^2 \sin^2\left(\frac{\alpha_{2T}}{2}\right) \quad (32)$$

$$\overline{a_{2P}b_{2P}} = \frac{d_2}{2\sin(\alpha_{2P}/2)} r_{2b} \quad (33)$$

$$A_{2Pt} = \frac{\pi}{2} (d_2 + d_{2P}) \overline{a_{2P}b_{2P}} = \frac{\pi}{2} \left[d_2 + 2r_{2b} \sin\left(\frac{\alpha_{2P}}{2}\right) \right] \left\{ \frac{d_2}{2\sin(\alpha_{2P}/2)} r_{2b} \right\} \quad (34)$$

$$\overline{a_{2T}b_{2T}} = \frac{d_2}{2\sin(\alpha_{2T}/2)} r_{2b} \quad (35)$$

$$A_{2Tt} = \frac{\pi}{2} (d_2 + d_{2T}) \overline{a_{2T}b_{2T}} = \frac{\pi}{2} \left[d_2 + 2r_{2b} \sin\left(\frac{\alpha_{2T}}{2}\right) \right] \left\{ \frac{d_2}{2\sin(\alpha_{2T}/2)} r_{2b} \right\} \quad (36)$$

$$Q_{2P} = C_d A_{2Pt} \sqrt{2(P_S - P_A)/\rho} \quad (37)$$

$$Q_{2T} = C_d A_{2Tt} \sqrt{2(P_A - P_T)/\rho} \quad (38)$$

2.5 Mathematical Model of the DCV-3

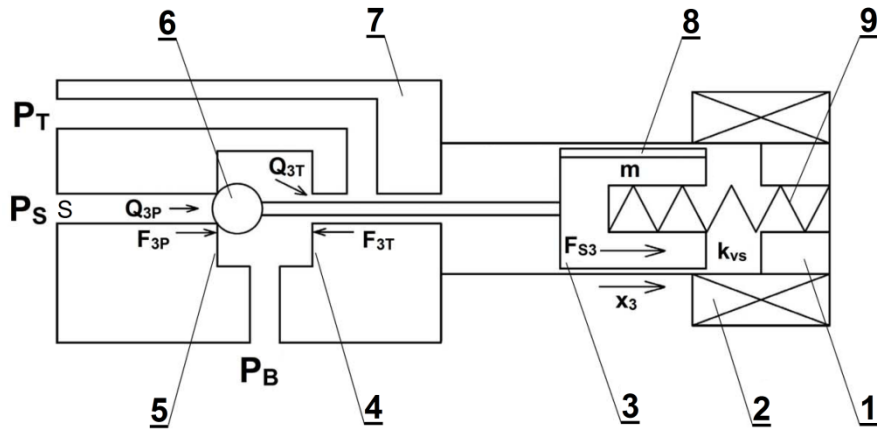


Fig. 8. Schematic diagram of the DCV-3

The following are the mathematical relations describing DCV-3 were deduced systematically from Figs. 8 and 9.

$$P_S A_{3Pp} - P_T A_{3Tp} + F_{3P} + F_{S3} - F_{3T} = m \ddot{x}_3 + f_v \dot{x}_3 + k_{vs} (x_3 + x_{o3}) \quad (39)$$

$$F_{3P} = \begin{cases} 0 & s_3 > x_3 > 0 \\ K_{sP} |x_3| - R_{sP} \frac{dx_3}{dt} & x_3 < 0 \end{cases} \quad (40)$$

$$F_{3T} = \begin{cases} K_{sT} |x_3 - s_3| + R_{sT} \frac{dx_3}{dt} & x_3 > s_3 \\ 0 & s_3 > x_3 > 0 \end{cases} \quad (41)$$

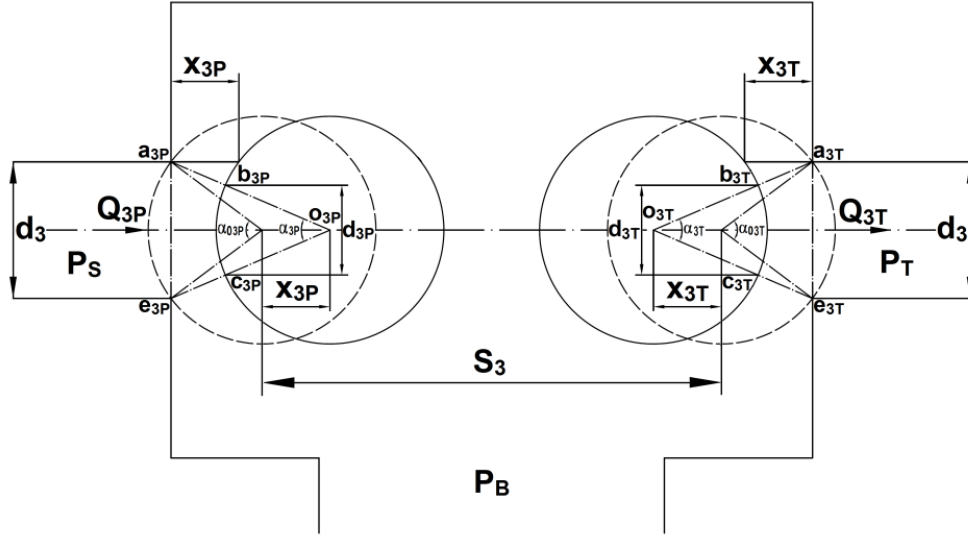


Fig. 9. Poppet valve dimensions and areas of the DCV-3

$$A_{3Ppm} = \frac{\pi}{4} d_3^2 \quad (42)$$

$$\alpha_{o3P} = 2 \sin^{-1} \left(\frac{d_3}{2r_{3b}} \right) \quad (43)$$

$$\alpha_{3P} = 2 \tan^{-1} \left[\frac{d_2}{2\{r_{3b} \cos(\alpha_{o3P}/2) + X_{3P}\}} \right] \quad (44)$$

$$d_{3P} = 2r_{3b} \sin \left(\frac{\alpha_{3P}}{2} \right) \quad (45)$$

$$A_{3Pp} = \frac{\pi}{4} d_{3P}^2 = \pi r_{3b}^2 \sin^2 \left(\frac{\alpha_{3P}}{2} \right) \quad (46)$$

$$A_{3Tpm} = \frac{\pi}{4} d_3^2 \quad (47)$$

$$\alpha_{o3T} = 2 \sin^{-1} \left(\frac{d_3}{2r_{3b}} \right) \quad (48)$$

$$\alpha_{3T} = 2 \tan^{-1} \left[\frac{d_3}{2\{r_{3b} \cos(\alpha_{o3T}/2) + X_{3T}\}} \right] \quad (49)$$

$$d_{3T} = 2r_{3b} \sin \left(\frac{\alpha_{3T}}{2} \right) \quad (50)$$

$$A_{3Tp} = \frac{\pi}{4} d_{3T}^2 = \pi r_{3b}^2 \sin^2 \left(\frac{\alpha_{3T}}{2} \right) \quad (51)$$

$$\overline{a_{3P}b_{3P}} = \frac{d_3}{2 \sin(\alpha_{3P}/2)} - r_{3b} \quad (52)$$

$$A_{3Pi} = \frac{\pi}{2} (d_3 + d_{3P}) \overline{a_{3P}b_{3P}} = \frac{\pi}{2} \left[d_3 + 2r_{3b} \sin \left(\frac{\alpha_{3P}}{2} \right) \right] \left\{ \frac{d_3}{2 \sin(\alpha_{3P}/2)} - r_{3b} \right\} \quad (53)$$

$$\overline{a_{3T}b_{3T}} = \frac{d_3}{2 \sin(\alpha_{3T}/2)} - r_{3b} \quad (54)$$

$$A_{3Ti} = \frac{\pi}{2} (d_3 + d_{3T}) \overline{a_{3T}b_{3T}} = \frac{\pi}{2} \left[d_3 + 2r_{3b} \sin \left(\frac{\alpha_{3T}}{2} \right) \right] \left\{ \frac{d_3}{2 \sin(\alpha_{3T}/2)} - r_{3b} \right\} \quad (55)$$

$$Q_{3P} = C_d A_{3Pt} \sqrt{2(P_S - P_B) / \rho} \quad (56)$$

$$Q_{3T} = C_d A_{3Tt} \sqrt{2(P_B - P_T) / \rho} \quad (57)$$

2.6 Continuity Equations

Continuity Equations Applied to the Inner Chamber (S)

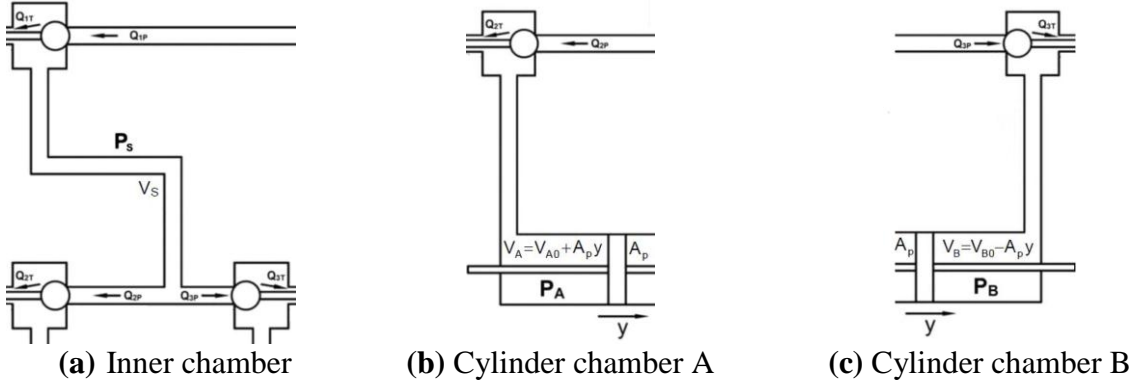


Fig.10. DCV assembly chambers

The application of the continuity equation to the inner valve chamber, Fig.10(a) yields:

$$Q_{1P} - Q_{1T} - Q_{2P} - Q_{3P} = \frac{V_S}{B} \frac{dP_S}{dt} \quad (58)$$

Continuity Equation Applied to the Cylinder Chamber (A)

The following equation is obtained by applying the continuity equation to the left cylinder chamber, Fig.10(b)

$$Q_{2P} - Q_{2T} - A_p \frac{dy}{dt} = \frac{V_A}{B} \frac{dP_A}{dt} \quad (59)$$

where;

$$V_A = V_{A0} + A_p y \quad (60)$$

Continuity Equation applied to the Cylinder Chamber (B)

The following is the continuity equation of fluid flow in the right cylinder chamber, Fig.10(c).

$$Q_{3P} - Q_{3T} + A_p \frac{dy}{dt} = \frac{V_B}{B} \frac{dP_B}{dt} \quad (61)$$

where;

$$V_B = V_{B0} - A_p y \quad (62)$$

2.7 Equation of Motion of the Piston

According Newton's second law the motion of the piston of the steering cylinder under the effect of the hydraulic pressure, rolling resistance and viscous friction forces and inertia of both of the rotating and moving parts is described by the following equation.

$$(P_A - P_B) A_P - f_{rr} W_f \sin \delta \frac{L_s}{r_{rm}} - f_{vp} \dot{y} - \frac{I_{zz}}{r_{rm}} \ddot{\delta} = m_p \ddot{y} \quad (63)$$

3. Simulation of the Steering Valve

Equations 1 through 63 describe the dynamic behavior of the studied hydraulic steering system. These equations were used to develop a computer simulation program using SIMULINK. The numerical values of the constructional and operational parameters were obtained by direct measurements on the system parts and from the data supplied by the manufacturer.

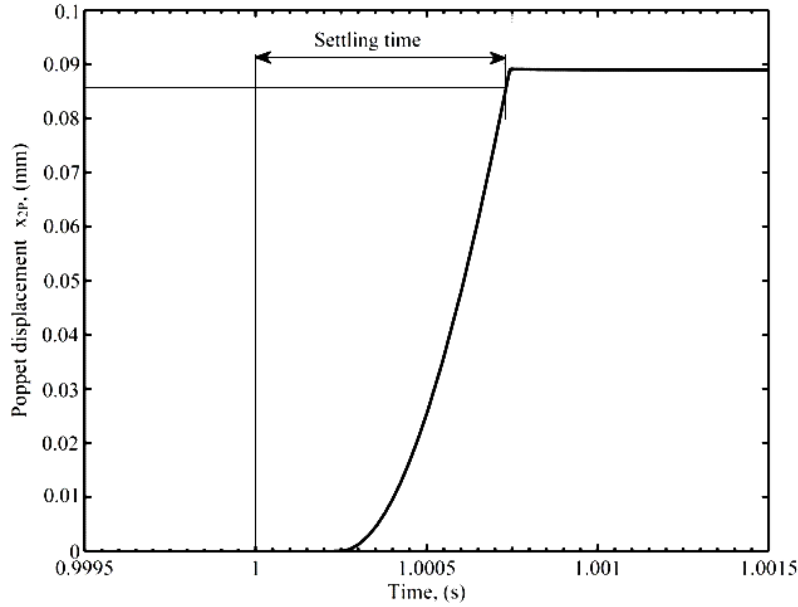


Fig. 11. Transient response of poppet displacement x_2 to step input of solenoid force $F_{S2} = 15$ N

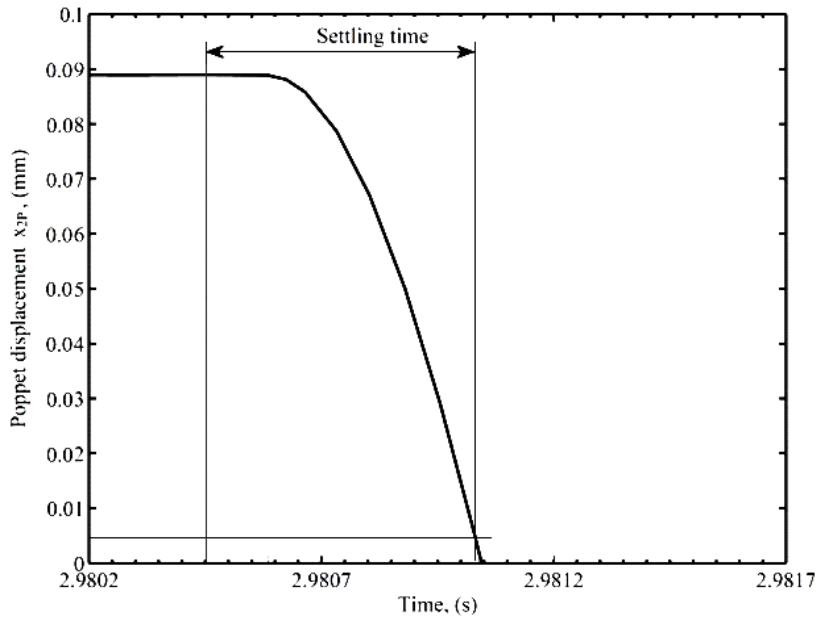


Fig.12. Transient response of poppet displacement x_2 to step reduction of force F_{S2} from 15 to 0 N

The transient displacement of the poppet of the DCV-2 was calculated for step application of solenoid force of 15 N, applied at time $t= 1$ s. The supply and return pressures were 20.68 and 0.59 MPa, respectively. The simulation result is shown in Fig. 11. This figure shows a delay time within 0.25 ms and a settling time within 0.75 ms. The delay time may be attributed to the very fine throttling and corresponding low flow rate, which causes the delay of building the required pressure difference across the steering cylinder piston, [7].

The transient response of the poppet displacement to step release of the solenoid force was also calculated, Fig. 12. The observable short settling time is attributed to the too small poppet stroke (0.09 mm), the high pressure forces and the very small poppet and plunger mass.

4. Validation of Simulation Program

In order to verify the obtained theoretical simulation results of the steering DCV model in steady state, its simulation program by SIMULINK has been run by applying several values of at pressure port (P_P), return port (P_T) pressure also changes accordingly and simulating the corresponding values of the valve flow rate. These experimental results have been plotted with the corresponding theoretical results in Figs. 13 and 14 respectively.

It is obvious from these plots that the theoretical simulation model of the DCV assembly agrees with the experimental results, the maximum deviation between the experimental and theoretical work is 8.56% full scale with an average error over the whole readings 5.27%.

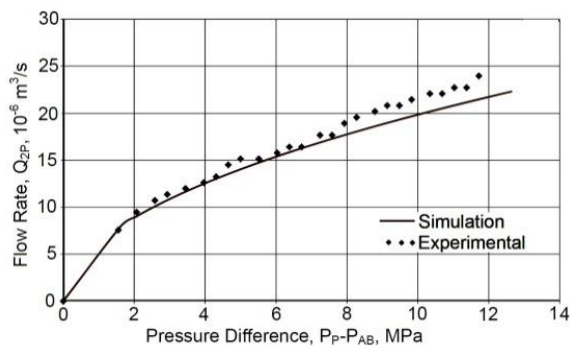


Fig.13. Experimental and simulation results of DCV-2 input flow rate

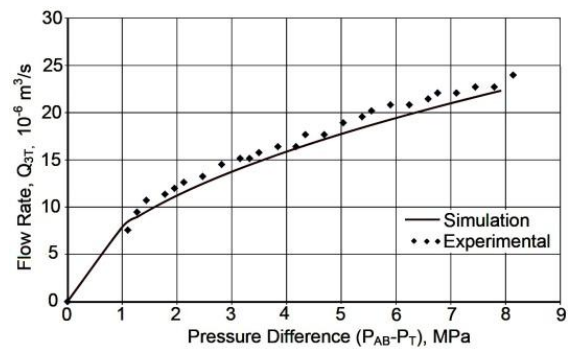
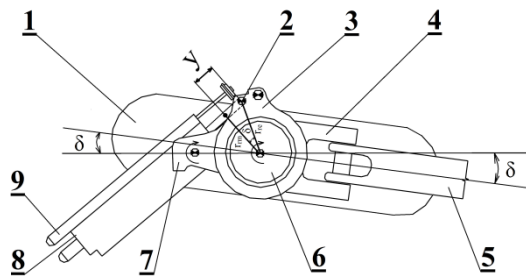


Fig.14. Experimental and simulation results of DCV-3 input flow rate

5. Mechanical System



1. Front wheel, 2. Rod end, 3. Bell crank, 4. Collar, 5. Torque arm, 6. Inner piston, 7. Upper bracket, 8. Steering cylinder, 9. Feedback potentiometer, 10. Lower bracket.

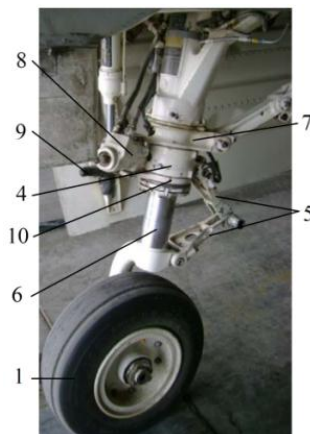


Fig.15. Front wheel steering mechanism

The mechanical parts of the studied vehicle steering system are illustrated in Fig.15. Steering cylinder pivot center is attached to the upper (7) and lower (10) brackets, allowing the cylinder (8) to rotate during transient position of the rod end (2) between extended and retracted positions. This design of the bell crank mechanism (3) allows transmitting the linear displacement (y) of the rod end to rotation in the collar (4) with angle (\square). The steering cylinder rod end (2) drives the collar (4) to rotate around the steering axis. The steering torque is transmitted to the front wheel through the torque arm (5) and the inner piston (6) of the shock strut. The angle (δ) is the steering angle with which the front wheel (1) rotates to the left and to the right. (r_{re}) is the radius between cylinder rod end (2) center and the shock strut center. As the rod end changes its position according to the magnitude and direction of the cylinder displacement (y), the magnitude of the steering load arm (r_{rm}) changes. The feedback potentiometer (9) is attached to the cylinder. The resistance of the feedback potentiometer varies according to the cylinder displacement.

Studying the steering system kinematics shows that the relation between the steering angle (δ) and piston-rod displacement (y) is practically linear over the actual operating range with accuracy 99.99 %, Eq. 64 and Fig. 16. The variation of the steering load arm (r_{rm}) and piston displacement (y) is obtained by least square curve fitting using MICROSOFT EXCEL with accuracy 99.94 % and the relation is given by Eq. 65 and Fig. 17.

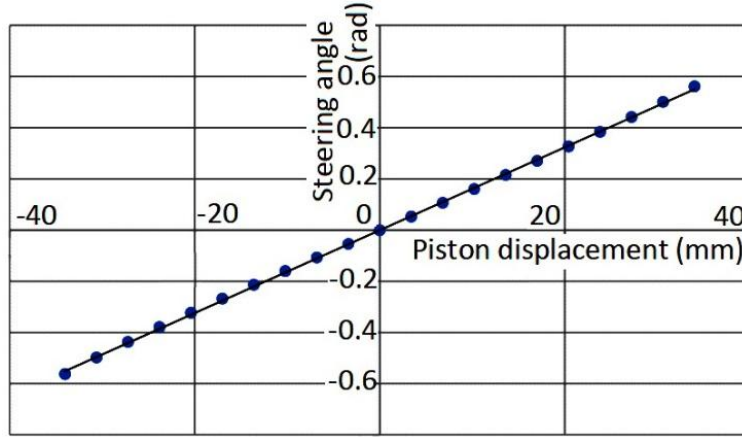


Fig. 16. Relationship between steering angle (δ) and piston displacement (y)

$$\delta = 16.1823 y \quad (64)$$

$$r_{rm} = 0.063 - 0.059 y - 5.969 y^2 + 51.51 y^3 - 2943 y^4 + 57234 y^5 \quad (65)$$

From Eq. 63, the reduced mass for both of the moving and rotating parts can be evaluated as follows:

$$m_{red} = m_p + \frac{I_{zz}}{r_{rm}} \ddot{\delta} \quad (66)$$

By substituting Eq. 64 in Eq. 66:

$$m_{red} = m_p + 16.1823 \frac{I_{zz}}{r_{rm}} \quad (67)$$

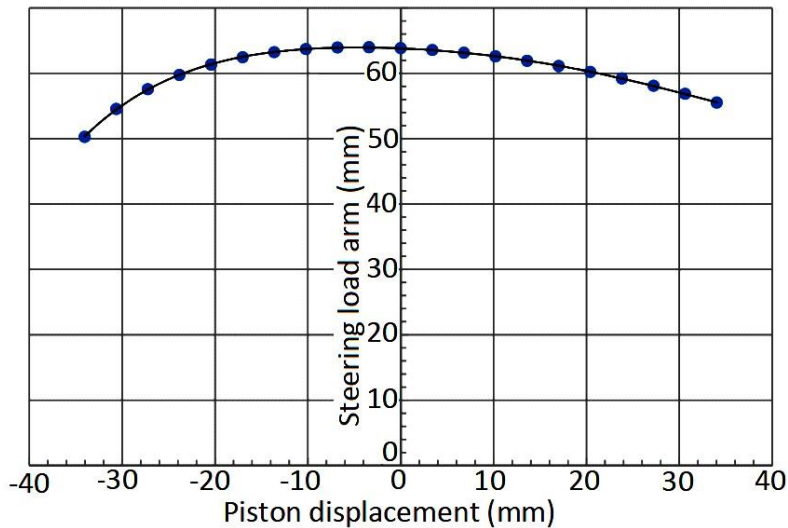


Fig. 17. Relationship between the steering load arm (r_{rm}) and the cylinder displacement (y)

Rolling resistance on hard surfaces is caused by hysteresis in the rubber of the tire. The pressure in the leading half of the contact patch is higher than in the trailing half, and consequently the resultant vertical force does not act through the middle of the wheel, [8]. A horizontal force in the opposite direction to the wheel movement is needed to maintain equilibrium. This horizontal force is known as the rolling resistance, [9]. The ratio of the rolling resistance in the front tire (F_{rf}), to vertical load (W_f), on the front tire is known as the coefficient of rolling resistance (f_{rr}). This can be described mathematically in Eq. 68 as follows:

$$F_{rf} = f_{rr} W_f \tag{68}$$

A value of ($f_{rr} = 0.02$) is typically used for this class of vehicle’s tires, [10].

The rolling resistance force (F_{rf}) doesn’t act at the center of the contact patch due to the caster angle Fig. 18, It affects at distance (L_s) in front of it. That makes the lever-arm of the rolling resistance is ($L_s \sin \delta$).

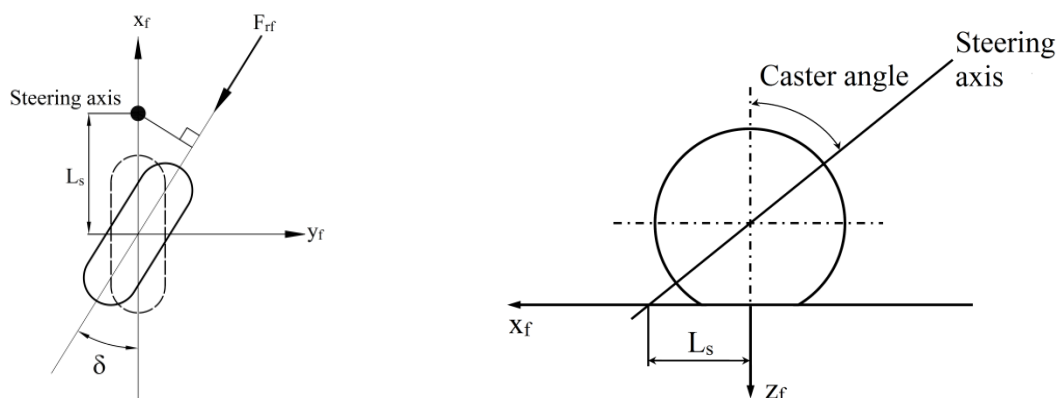


Fig. 18. The effect of rolling resistance on a steering tire

6. Transient Response of the Steering System

The transient response of the steering cylinder displacement was calculated for step pedal displacements of different magnitudes. The calculation results are given by Fig.19. This figure shows that the steering system operates most of the time at constant speed. This is

attributed to the full opening of the DCVs. The valves close on reaching the required position. By de-energizing the electric solenoids E1 and E2. The steering cylinder speed was measured. The experimental results showed good agreement with the simulation results.

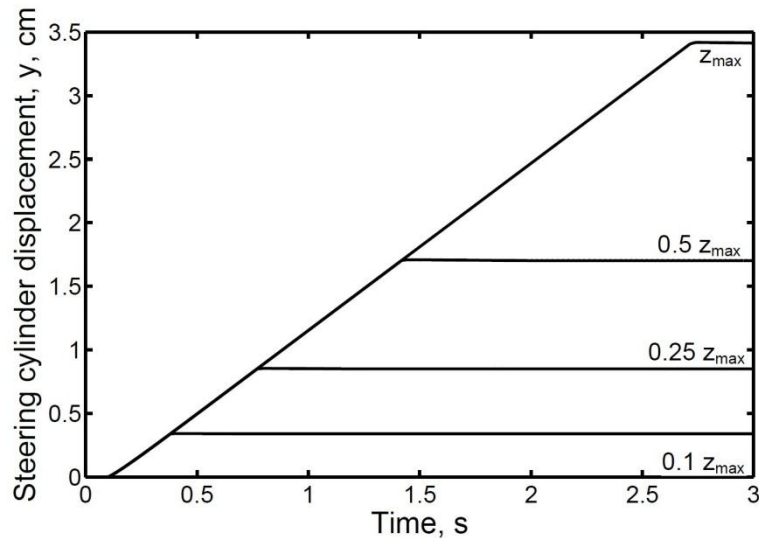


Fig.19. Transient response of the unloaded steering cylinder to step inputs of different magnitudes

7. Conclusions

This paper deals with the investigation of the dynamic performance of a peculiar steering system. This system is used for a three-wheeled vehicle and is built using hydraulic directional control valve assembly. The system was studied theoretically by deducing a describing mathematical model and developing a computer simulation program. Meanwhile the steering valve flow rates and steady state steering cylinder speed were measured. The experimental and simulation results showed good agreement, which validates the valve simulation results in the steady state.

The theoretical analysis of the transient response showed very fast response. This high speed of response is due to the short poppet stroke (0.09 mm) and its small dimensions and mass (1 mm radius).

This developed model will be used to investigate the dynamic behavior of the studied vehicle during steering.

8. References

- [1] Klyde, D.H., Magdaleno, R.E. and Reinsberg, J.G., "The Effect of Tire Pressure on Vehicle Ground Handling". AIAA Paper No. 2002-4798 presented at the Atmospheric Flight Mechanics Conference, Monterey, CA. 2002.
- [2] Tayea, M.S., Emam, M.A., Shaaban, S.M., El-Demerdash, S.M. and M.G. Rabie, "Dynamic Performance of Electro-hydraulic Steering System for Off-road Vehicles", Int. J. of Vehicle Structures & Systems, Chennai, India, Volume 4, Issue 1, 2012, ISSN: 0975-3060 pp 1-9
- [3] Ibrahim, S.Y., Rabie, M.G. and Lotfy, A.H., "Experimental and Theoretical Investigation of the Performance of the Servo-actuator of a Hydraulic Power Steering System", Proceedings of the 8th AMME Conf., M.T.C., Cairo, May 1998, pp 395-407.
- [4] Joseph, D., "Automakers prepare for by-wire revolution", Design News, pp. S9-S16, 2001.
- [5] Hagga, S., "Development of fault-tolerant steer-by-wire system for earth moving equipment". PhD dissertation, university of Illinois at Chicago, Chicago, IL, 2002.

- [6] Rabie, M.G., “Fluid Power Engineering”, McGraw-Hill Professional, NY, USA, 2009.
- [7] Rabie, M.G., “Automatic Control for Mechanical Engineers”, ISBN 977-17-9869-3, 2010.
- [8] Rankin, J., “Bifurcation Analysis of Nonlinear Ground Handling of Vehicle”, Department of Engineering Mathematics, University of Bristol, A dissertation submitted to the University of Bristol in accordance with the requirements of the degree of Doctor of Philosophy in the Faculty of Engineering, 2010.
- [9] Wong, J.Y., “Theory of ground vehicles”, 3rd ed., Wiley-Interscience, 2001.
- [10] Mitchell, D.J., “Calculation of ground performance in take-off and landing”, Data Sheet 85029, ESDU, 1985.